

High-pressure reaction profiles and activation volumes of 1,3-cyclohexadiene dimerizations computed by the extreme pressure-polarizable continuum model (XP-PCM)

Bo Chen,^{1,2,*} K. N. Houk,³ and Roberto Cammi^{4,*}

¹ Donostia International Physics Center, Paseo Manuel de Lardizabal, 4, 20018 Donostia-San Sebastian, Spain

² IKERBASQUE, Basque Foundation for Science, Plaza Euskadi 5, 48009 Bilbao, Spain

³ Department of Chemistry and Biochemistry, University of California, Los Angeles, California 90095, United States

⁴ Department of Chemical Science, Life Science and Environmental Sustainability, University of Parma, Viale Parco Area delle Scienze. 17/a, Parma, 43100, Italy

bo.chen@dipc.org; roberto.cammi@unipr.it

Abstract

Quantum chemical calculations are reported for the thermal dimerizations of 1,3-cyclohexadiene at 1 atm and high pressures up to 6 GPa. Previous experiments [Klärner *et al. Angew. Chem. Int. Ed.* **1986**, *25*, 108], based on measured activation energies and activation volumes, suggested concerted mechanisms for the formation of the *endo* [4+2] cycloadduct and a [6+4]-ene adduct, and stepwise mechanisms for the formation of the *exo* [4+2] cycloadduct and two [2+2] cycloadducts. Computed activation enthalpies (ω B97XD, CCSD(T) and SC-NEVPT2) of plausible dimerization pathways at 1 atm agree well with the experiment activation energies and the values from previous calculations [Ess *et al. J. Org. Chem.* **2008**, *73*, 7586]. High-pressure reaction profiles, computed by the recently-

developed extreme pressure-polarizable continuum model (XP-PCM), show that the reduction of reaction barrier is more profound in concerted reactions than in stepwise reactions, which is rationalized on the basis of the volume profiles of different mechanisms. A clear shift of the transition state towards the reactant by high pressure is revealed for the [6+4]-ene reaction by the calculations. The computed activation volumes by XP-PCM agree excellently with the experimental values, confirming the existence of competing mechanisms in the thermal dimerizations of 1,3-cyclohexadiene.

Introduction

The rates of chemical reactions are usually affected by both temperature and pressure. The effect of temperature on the rate of a chemical reaction is measured as the activation energy.^{1,2} For thermally activated reactions (no tunneling³ involved), the larger the activation energy E_a , the greater the increase in the reaction rate with temperature.⁴ Activation energies are measured experimentally by treating the temperature dependence of the rate constant using the Arrhenius equation. The activation energy is the slope of the plot of $\ln k$ vs $1/T$, $E_a = R \left(\frac{\partial \ln k}{\partial (1/T)} \right)_p$, where k is the rate constant, T the temperature, R the ideal gas constant, and p the pressure.

The effect of pressure on the rate of a chemical reaction is measured by the volume of activation (or activation volume) ΔV^\ddagger .^{5,6,7,8,9,10,11,12,13,14,15,16,17,18} The volume of activation is the volume change of a reaction system from the reactant(s) to the transition state. Experimentally, activation volumes are obtained by studying the pressure dependence of the rate constants using $\Delta V^\ddagger = \left(\frac{\partial \Delta G^\ddagger}{\partial p} \right)_T = -RT \left(\frac{\partial \ln k}{\partial p} \right)_T$, where ΔG^\ddagger is the Gibbs energy of activation, according to the thermodynamic formulation of the transition state theory.^{4,19,20,21,22}

While activation energies are almost always positive,²³ activation volumes can commonly be both positive and negative. Reactions with negative and positive ΔV^\ddagger are accelerated and decelerated by pressure, respectively. Usually, the signs of activation volumes can be intuitively predicted. For example, in the case of a bond formation reaction

between two molecules (Figure 1), a negative ΔV^\ddagger is expected since the unimolecular transition state is more compact and hence has a smaller volume than the two separated reactant molecules. The opposite is usually true for bond cleavage reactions.

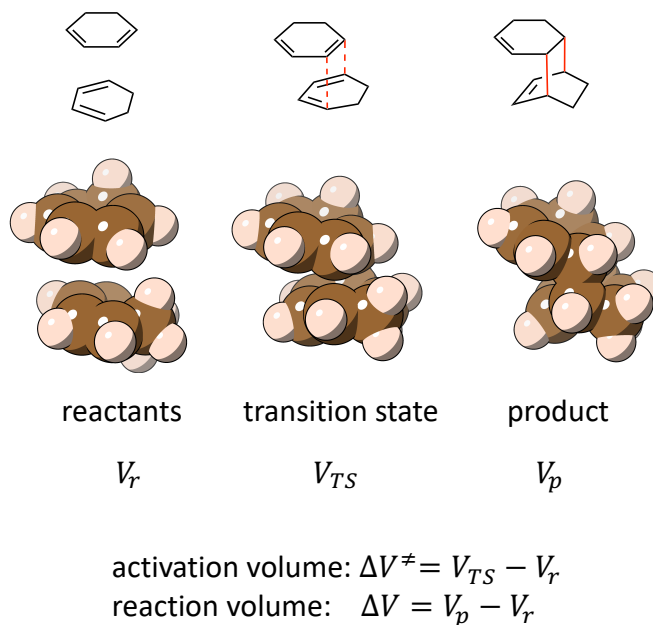


Figure 1. Schematic illustration of the activation volume and reaction volume (both are negative) of a Diels-Alder dimerization of 1,3-cyclohexadiene.

Measurements of ΔV^\ddagger are a valuable tool to distinguish different reaction mechanisms. A notable example is the case of several Diels-Alder reactions whose activation volumes have given evidences in favor of a concerted one-step mechanism over the competing two-step mechanism.^{24,25} Another exemplary case of competing mechanisms is revealed by the illuminating study of the effect of pressure on the thermal dimerization of 1,3-cyclohexadiene by Klärner et al in 1986.²⁶

At 1 atm, thermal dimerization of 1,3-cyclohexadiene yielded five reaction products—two [4+2] cycloadducts of the *endo* and *exo* configurations, two [2+2] cycloadducts of the *syn* and *anti* configurations, and one [6+4]-ene adduct (Figure 2). It was also observed that, under pressure up to 7 kbar, the reactions producing all five products

are accelerated, indicating negative activation volumes for all these reactions. Considering the bond-formation nature of these reactions, the observed acceleration under pressure is not surprising.

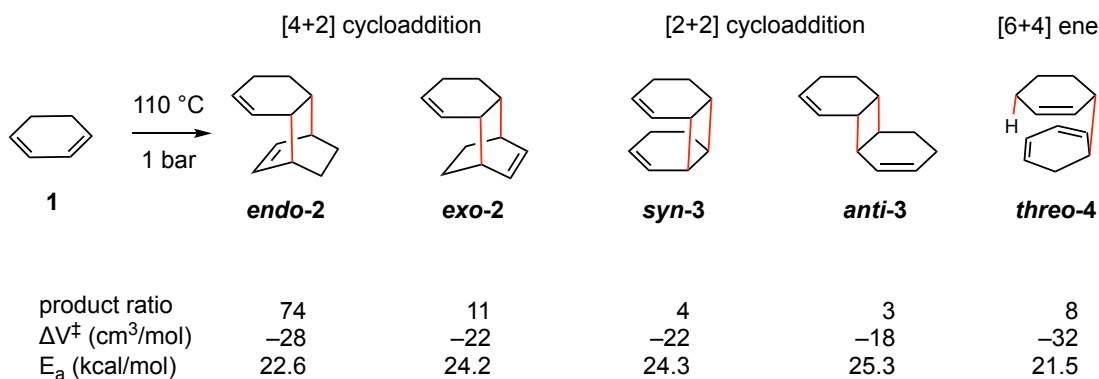
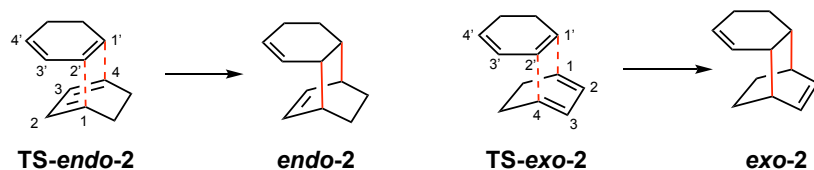


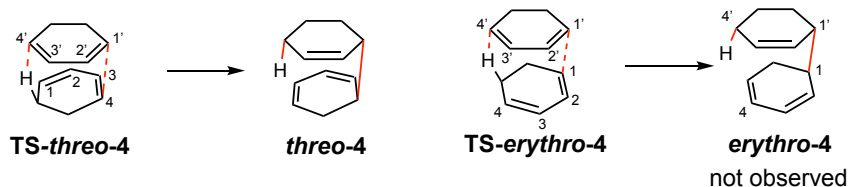
Figure 2. The observed products of thermal dimerizations of 1,3-cyclohexadiene. New bonds are in red. Experimentally measured activation volumes (ΔV^\ddagger) and activation energies (E_a) are shown.

Apparently, different mechanisms are in operation in this dimerization, for both the symmetry-allowed [4+2] and [6+4] and forbidden [2+2] dimers, according to the Woodward-Hoffmann rules,²⁷ were observed. The symmetry-allowed [4+2] cycloadducts and the [6+4]-ene adduct could, in principle, be formed through either a concerted or stepwise mechanism, whereas the symmetry-forbidden [2+2] cycloadducts are usually expected to be formed via a stepwise mechanism under thermal conditions (Figure 3).^{26,28} The main difference between the concerted and stepwise mechanisms, in terms of activation volume, is that two bonds are formed at once in a concerted mechanism and only one bond is initially formed in a stepwise mechanism, so that the concerted transition state (TS) structure is usually more compact than the stepwise TS structure. Therefore, the concerted reaction usually has a more negative activation volume than a stepwise reaction.

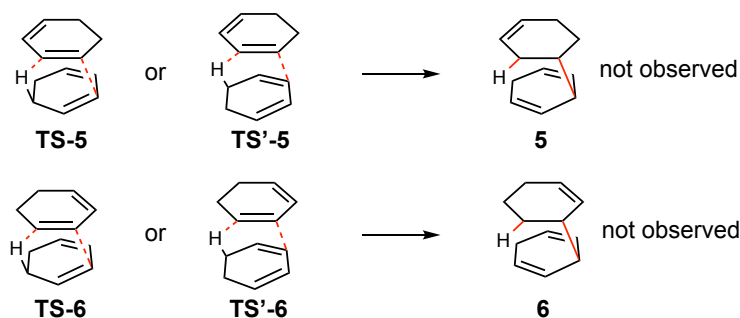
Concerted [4+2]-cycloaddition pathways



Concerted [6+4]-ene pathways



Concerted [4+2]-ene pathways



Stepwise pathways

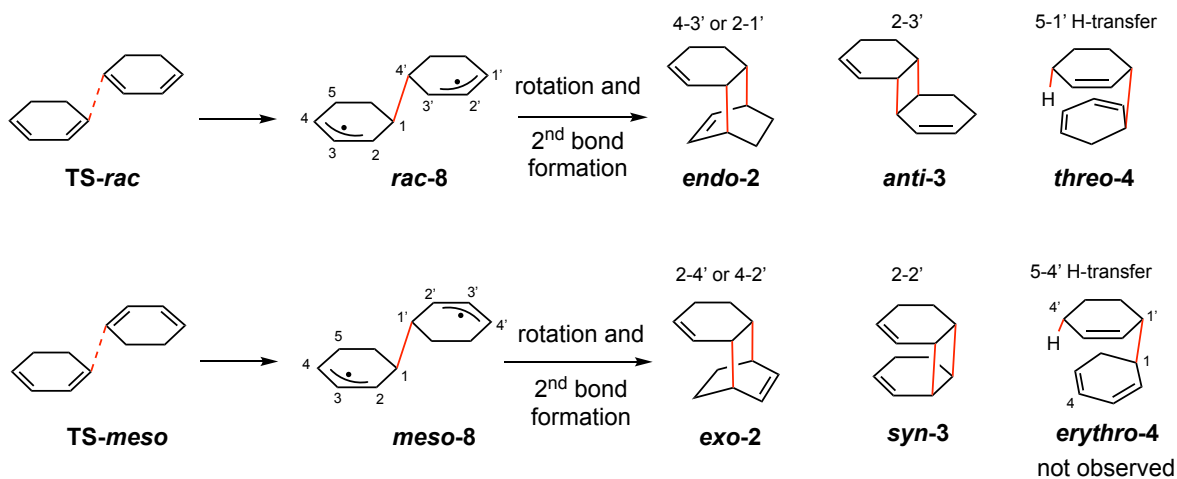


Figure 3. Plausible concerted and stepwise mechanisms. The ring position numbering of 1,3-cyclohexadiene follows a clockwise fashion, with primed and unprimed numbers for different rings.

Klärner et al.²⁶ observed (Figure 2) that the reactions yielding the *endo* [4+2]-cycloadduct and the *threo* [6+4]-ene adduct were accelerated the most by pressure. Measurements of volumes of activation show that the reaction leading to **endo-2** has $\Delta V^\ddagger = -28 \text{ cm}^3/\text{mol}$ and the reaction leading to **threo-4** has $\Delta V^\ddagger = -32 \text{ cm}^3/\text{mol}$. The reactions leading to the other three observed products have smaller ΔV^\ddagger between -22 and $-18 \text{ cm}^3/\text{mol}$.

Based on these ΔV^\ddagger data, Klärner et al.²⁶ reasoned that **endo-2** and **threo-4** are most likely formed by concerted mechanisms because their relatively large and negative volumes of activation suggest highly compact TS structures. On the other hand, the other three reactions with less negative activation volumes are more compatible with stepwise mechanisms. Interestingly, the reactions affording the [4+2]-adduct **exo-2** and [2+2]-adduct **syn-3** were measured to have essentially the same activation volume and activation energy, which led Klärner et al. to argue that these two reactions likely follow a common stepwise mechanism.

The measured activation energies E_a for the reactions giving the five products in Figure 2 are within 4 kcal/mol. An even smaller difference in E_a is seen between the *endo* and *exo* [4+2]-cycloadditions, though the former likely follows a concerted mechanism while the latter a stepwise mechanism, based on the measured difference in ΔV^\ddagger .²⁶ Interestingly, it seems that the more negative the ΔV^\ddagger , the lower the E_a of the reaction, though the two quantities do not necessarily have a correlation.

In 2008, Ess *et al.* calculated the TS structures and reaction pathways for the dimerization of 1,3-cyclohexadiene in the gas-phase.²⁸ Calculations at B3LYP, CASPT2 and CBS-QB3 levels show that the computed reaction barriers for the concerted [4+2]-cycloadditions, concerted [6+4]-ene reactions, and the stepwise additions (Figure 3) are within 5 kcal/mol. This small difference is consistent with the difference in experimental E_a , confirming the competitive nature of the concerted and stepwise mechanisms. However, the exact energetic order of these TS structures is slightly different between the calculation and experiment.

The Ess *et al.* work focused on the activation energies and didn't deal with the activation volumes of the reaction. Theoretical calculations of ΔV^\ddagger , especially from first-principles, have been a challenge. A simple and intuitive way to compute ΔV^\ddagger is to calculate the difference in van der Waals (vdW) volumes of the molecule at the reactant and transition states. The vdW volume is the volume of interlocking vdW spheres (often with scaled vdW radii) centered on the constituting atoms of the molecule. However, likely due to the negligence of intermolecular interactions and solvent effect, ΔV^\ddagger computed by this method are always too small in magnitude. An empirical packing coefficient was introduced to account for such negligence and to correct the underestimated ΔV^\ddagger , computed by this method.^{15,29}

A new method for more rigorous ΔV^\ddagger calculations is the recently-developed extreme pressure polarizable continuum model (XP-PCM).³⁰ As an extension of the popular polarizable continuum model (PCM) that tackles molecular solution energies at the standard condition of pressure, the XP-PCM allows for quantum chemical calculations of the energy profiles of chemical reactions under pressure. The effect of the pressure is introduced in XP-PCM via a repulsive interaction between the reactive molecular system and the surrounding solvent medium. Within XP-PCM, ΔV^\ddagger can be computed, according to the transition state theory, as the derivative of activation free energy with respect to pressure. The XP-PCM method has been applied to the calculations of the energy profiles of a subset of pericyclic reactions.^{17,31} Interesting phenomena such as a shift of the transition state and a switch of the rate determining step have been discovered by the calculations.¹⁷ Furthermore, the computed ΔV^\ddagger are in reasonable agreement with experimental value.¹⁷ Recent work by Fukuda and Nakatani applied the XP-PCM method to a retrocycloaddition.³² The necessary details of the physical basis and computational protocol of the XP-PCM method are given in the Computational Methodology section. In addition to reaction profiles, the XP-PCM method has also been applied to the studies of the effect of pressure on a variety of molecular properties, such as equilibrium geometries,^{33,34,35} vibrational frequencies,^{36,37,38} electronic excitation energies.³⁹

We note here relevant approaches derived from the mechanochemistry field for high-pressure calculations on molecules and reactions.^{40,41,42,43} Notably, the recent

GOSTSHYP method from the Stauch group⁴⁴ is capable of calculating activation volumes of reactions. Another approach for simulating high-pressure organic reactions employs a simulation box with periodic boundary condition, filled with solvated reactant molecules. The solvent molecules are explicitly included in the simulation box, in contrast to the implicit solvation approach in the XP-PCM method. Molecular dynamics (MD) simulations or Monte Carlo simulations (an early example by Klärner et al.²⁵) are performed to obtain reaction profiles at high pressures and activation volumes. Due to the large size of the system using a simulation box, the MD simulations were usually done with force fields, as illustrated in the works from the Weinberg group,^{45,46,47,48} or by a hybrid quantum mechanics/molecular mechanics (QM/MM) approach, as shown in the work by Plotnikov and Martinez⁴⁹ and a recent work by Loco *et al.*⁵⁰

We now report a thorough consideration of the potential energy surface (PES) of the thermal dimerization 1,3-cyclohexadiene, including [4+2]-ene pathways that were not considered previously. In addition, we report, for the first time, XP-PCM calculations on the activation volumes for the various dimerization reactions of 1,3-cyclohexadiene, offering a new approach for computationally studying the competing mechanisms of this reaction.

Computational Methods

Gas-phase calculations. Gas-phase geometries were optimized at the ω B97XD⁵¹/def2-TZVP⁵² level of theory. Frequency analyses were performed at the same level to verify the optimized structure to be either a minimum or a transition state, and to obtain the zero-point vibrational, thermal, and entropic corrections, necessary in calculating enthalpies and free energies. For open-shell singlets that appear in the stepwise mechanism, broken-symmetry DFT with spin-projection by the Yamaguchi-Houk procedure⁵³ was used. On the ω B97XD/def2-TZVP optimized structures, single-point calculations were performed using the strongly contracted N-electron valence state perturbation theory (SC-NEVPT2)^{54,55,56} and coupled-cluster CCSD(T)^{57,58} methods with the same def2-TZVP basis set. In the SC-NEVPT2 calculations, a (4,4) active space was used for

1,3-cyclohexadiene, which comprises the valence π -type orbitals and the valence π electrons in the molecules. An (8,8) active space was used for the transition states, which consists of the same set of π -type orbitals and π electrons of two molecules of 1,3-cyclohexadiene; however, some of the π -type orbitals become more of σ -type orbitals in the bond formation regions in the transition states. The ω B97XD and CCSD(T) calculations were computed using the Gaussian 16⁵⁹ program package. The SC-NEVPT2 calculations were done with the ORCA 4.2.1^{60,61} program package.

High-pressure calculations. High pressure calculations were performed using the XP-PCM method at the ω B97XD/def2-TZVP level of theory in Gaussian 16 and an in-house Julia script. The XP-PCM is a quantum chemical method aimed to introduce the effects of the pressure on the calculation of the electronic energy G_{er} of a molecular system in a dense medium via a Pauli exchange-repulsion interaction between the molecular system and the external medium. Such a Pauli-exchange repulsion is motivated by the fact that at high pressure, the reduction of the volume of a dense medium forces the intermolecular distances below the van der Waals contacts, in a domain where the intermolecular interactions are dominated by the Pauli exchange-repulsion.⁶² The increase of the pressure is modeled by simply shrinking the volume V_c of the cavity hosting the molecular system so as to increase the overlap between the electron densities of the system and of the external medium (Figure 4). This molecular cavity is built up starting from the envelope of vdW spheres centered on the nuclei of the reactive system and with scaled vdW radii.

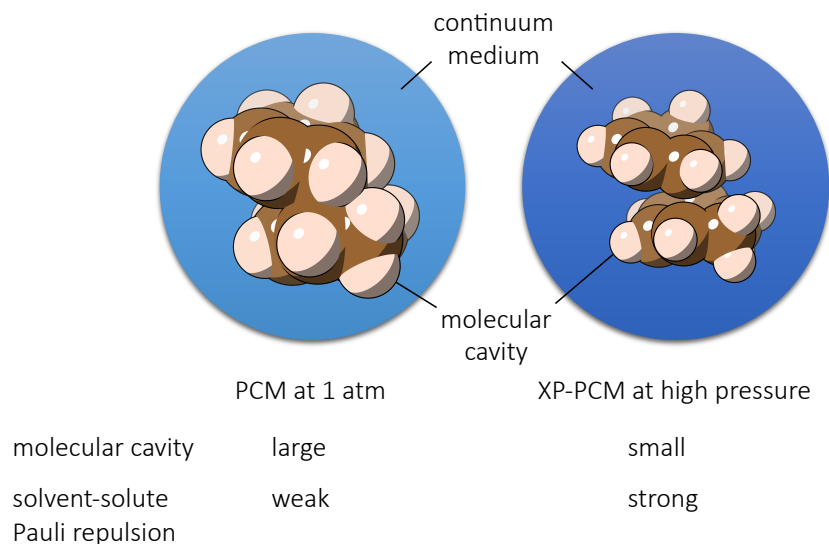


Figure 4. The XP-PCM model as an extension of the PCM model. A molecular system is confined in a molecular-shaped cavity (in this case the vdW cavity) in the external medium (in blue). The combination of a smaller size of the cavity and a stronger solvent-solute Pauli repulsion in XP-PCM models the effect of compression on the molecule.

In studying chemical reactions at high pressure, the effective potential energy for the motion of the nuclei of the reactive system, $G_{tot}(p)$, corresponds to the electronic energy $G_{er}(p)$, supplemented by a contribution of the so-called cavitation Gibbs energy that corresponds to the work necessary to create the void cavity hosting the molecular solute at the given condition of pressure p :

$$G_{tot}(p) = G_{er}(p) + G_{cav}(p). \quad (1)$$

This work also includes a configurational entropic contribution from the external medium.⁶³ The effective potential energy profile for a reaction at a given pressure p is then determined by computing $G_{tot}(p)$ for a set of selected structures along a suitable reaction coordinate. According to the transition state theory, the activation volume ΔV^\ddagger is determined from the slope of the corresponding activation energy $\Delta G_{tot}^\ddagger(p)$ as a function of the pressure,

$$\Delta V^\ddagger = \Delta G_{tot}^\ddagger(p)/dp. \quad (2)$$

In this work, the effective potential energy profile for a reaction at a given pressure p is then determined by computing $G_{tot}(p)$. The corresponding activation volume ΔV^\ddagger is computed by the same computational protocol used previously for the study of the effect of pressure on a selection of pericyclic reactions, where reasonable agreement of the computed activation volumes with experiment values was obtained.¹⁷ We recommend that interested readers consult ref 17 and the SI of the current paper for a detailed tutorial about the protocol. All the XP-PCM calculations are performed for selected structures (reactants, transition state, product) along the gas phase intrinsic reaction coordinates.

Potential energy surface at 1 atm

Mechanisms considered. As shown in [Figure 3](#), the concerted pathways considered in this paper include [4+2]-cycloadditions, [6+4]-ene reactions, and [4+2]-ene reactions. The [4+2]-ene pathways were not considered in previous calculations by Ess *et al.*²⁸ For the concerted [4+2]-cycloadditions and [6+4]-ene reactions, each of these pathways can generate two stereo isomers as a result of different relative orientations of the two cyclohexadiene rings in the TS structures. These isomers are termed *endo* and *exo* for the [4+2] cycloaddition adducts and *threo* (also could be called *rac* or *dl*) and *erythro* (also could be called *meso*) for the [6+4] ene-adducts.

For concerted [4+2]-ene reactions, two pathways are possible. In each of them, there exist configurational isomers for the TS, for example, **TS-5** and **TS'-5**. However, both of these two TS structures lead to the same dimer (i.e., **5**). The configurational isomerism in the TS disappears in the dimer because the bottom ring in the adduct becomes 1,4-cyclohexadiene that does not contain any stereocenter.

For stepwise pathways, we considered those beginning with a C–C bond formation between two 1,3-hexadiene molecules at the terminus of the diene moieties and generating a diallyl intermediate, *rac-8* or *meso-8*. Either of the two intermediates contains two stereocenters, but the *meso-8* isomer is achiral due to the presence of an inversion center in the structure. Other stepwise pathways involving bond formation at internal sites of the

diene moiety are likely to be unfavorable due to the generation of isolated (i.e., not in conjugation with a double bond) radical sites; these pathways are not considered. In the second step, a rotation about the first formed C–C bond followed by a radical recombination or a H-transfer leads to a cycloaddition or ene product. For example, a clockwise rotation of the top ring in **rac-8** intermediate ~60 degrees about C1–C4' and radical recombination at C2 and C3' generate **anti-3**. A rotation of the same ring ~120 degrees and C4–C3' radical recombination yield **endo-2**. A further clockwise rotation (~150 degrees) bringing C5 and C1' in proximity could allow H-transfer from C5 to C1', leading to the ene product **threo-4**. Similar analysis for **meso-8** shows that **exo-2**, **syn-3** and **erythro-4** can be formed from it, though **erythro-4** was not observed experimentally.

Concerted [4+2] cycloadditions vs [6+4]-ene reactions. Figure 5 shows the potential energy surface of various dimerization pathways of 1,3-cyclohexadiene at 1 atm, calculated at the ω B97XD/def2-TZVP level of theory. Table 1 reports the computed reaction barriers at ω B97XD, multireference perturbation NEVPT2, and coupled-cluster CCSD(T) levels.

Concerted pathways

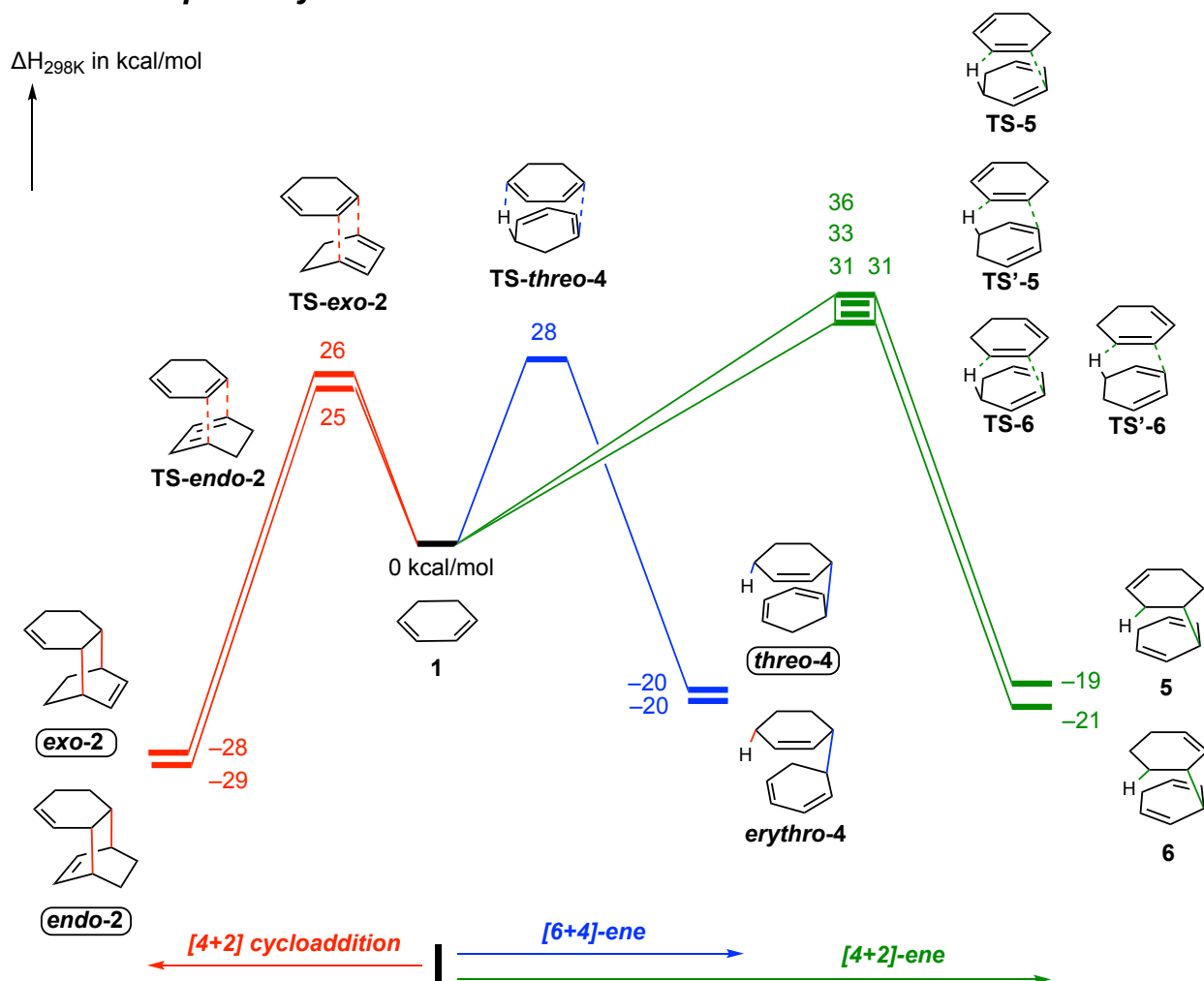


Figure 5. 1 atm enthalpic profiles of concerted pathways calculated at the ω B97XD/def2-TZVP level of theory. Experimentally-observed dimers are indicated by rounded-corner boxes around the labels. 3D drawings of the transition states are given in the Supporting Information.

At the ω B97XD/def2-TZVP level of theory, the *endo* [4+2] cycloaddition pathway going through **TS-endo-2** is calculated to have the lowest enthalpic barrier of 25 kcal/mol. The barrier of the *exo* pathway is 1 kcal/mol higher, likely due to the absence of secondary orbital interactions⁶⁴ in **TS-exo-2**. ω B97XD/def2-TZVP calculations also show that the activation enthalpy of the *threo* [6+4]-ene reaction going through **TS-threo-4** is 3 kcal/mol higher than that of the *endo* [4+2] cycloaddition. However, CCSD(T)/def2-TZVP single-

point calculations give opposite results that the *threo* [6+4]-ene pathway is the most favored pathway, with **TS-*threo*-4** being 1 kcal/mol lower than **TS-*endo*-2**. The CCSD(T) computed activation enthalpies agree excellently with the experimental activation energies (Table 1).

Table 1. Calculated activation enthalpies ΔH_{298K}^\ddagger and Gibbs activation energy ΔG_{298K}^\ddagger (in parenthesis), and experimental activation energies E_a and pre-exponential factor lgA of the Arrhenius Equation for the five dimerization mechanisms of cyclohexadiene. Zero-point vibrational, thermal, and entropic corrections are computed at the ω B97XD/def2-TZVP level. For the stepwise TS structures, the arrow “ \rightarrow ” points from spin-unprojected to spin-projected energies. All energies are in kcal/mol.

Mechanism	TS structure	Calc. ΔH_{298K}^\ddagger (ΔG_{298K}^\ddagger) in kcal/mol			Expt. E_a in kcal/mol	Expt. lgA
		ω B97XD ^a	NEVPT2 ^b	CCSD(T) ^c		
Concerted [4+2]	TS-<i>endo</i>-2	25 (38)	18 (31)	22 (34)	22.6	5.46
Concerted [4+2]	TS-<i>exo</i>-2	26 (40)	20 (34)	24 (37)	n.a.	n.a.
Concerted [6+4]-ene	TS-<i>threo</i>-4	28 (42)	18 (33)	21 (35)	21.5	3.87
Stepwise	TS-<i>meso</i>	24 (36) \rightarrow 18 (30) ^d	19 (31)		24.2/24.3	5.51/5.10
Stepwise	TS-<i>rac</i>	28 (40) \rightarrow 21 (34) ^e	24 (37)		25.3	5.52

^a (U) ω B97XD/def2-TZVP; ^b NEVPT2(8,8)/def2-TZVP// (U) ω B97XD/def2-TZVP; ^c CCSD(T)/def2-TZVP// ω B97XD/def2-TZVP; ^d $\langle S^2 \rangle = 0.62$; ^e $\langle S^2 \rangle = 0.73$;

Interestingly, although both experiments and calculations show that the concerted [6+4]-ene reaction (via **TS-*threo*-4**) has the lowest activation energy/enthalpy, the corresponding [6+4]-ene adduct ***threo*-4** is only a minor product, comprising 8% of the observed dimers. Importantly, the product ratio does not change over the reaction course and all dimers are verified to be kinetically persistent, i.e., no interconversion among the dimers.²⁶ Therefore, the low product ratio of ***threo*-4** must mean that the [6+4]-ene reaction is relatively slow. Since the rate of a reaction is determined by ΔG^\ddagger , not just by ΔH^\ddagger or E_a , the two observations—the lowest activation energy/enthalpy and a relatively slow

reaction rate—about the [6+4]-ene reaction can be reconciled by realizing that this reaction has a significantly smaller activation entropy, compared with other reactions. Calculations show that the entropy of **TS-threo-4** is 5 J/mol·K smaller than **TS-endo-2**; this entropic difference corresponds to a difference of 1.5 kcal/mol in ΔG_{298K}^\ddagger , in favor of **TS-endo-2**. Inclusion of the entropic contribution to the Gibbs activation energy reverses the kinetic preference of [6+4]-ene reaction and [4+2] cycloaddition. The smaller entropy of **TS-threo-4** indicates higher structural order, a feature that also relates to the large negative activation volume of the [6+4]-ene reaction. We will discuss the compact geometry of **TS-threo-4** in a later section. The difference in activation entropy is also reflected by the pre-exponential factor of the Arrhenius equations for these reactions, according to the thermodynamic formulation of the transition state theory.^{4,19,20,21,22} Consistent with the computed smaller entropy of **TS-threo-4**, the [6+4]-ene reaction was experimentally measured to have a significantly smaller pre-exponential factor of the Arrhenius equation ($\lg A = 3.87$), compared with other reactions ($\lg A > 5$).

The [4+2] cycloadducts are computed to be the most thermodynamically stable ones among the 1,3-cyclohexadiene dimers considered. The [6+4]-ene adduct **threo-4** is about 10 kcal/mol less stable, but was observed to be kinetically persistent at 70 °C up to 3 kbar as well as at 110 °C and 1 atm.²⁶ At elevated temperature (161 °C), **threo-4** does slowly disproportionate into benzene and cyclohexene; a retro-[4+2]-ene mechanism was proposed for this disproportionation.²⁶ Our CCSD(T) calculations (in the supporting information) show that the TS structure of this disproportionation has a high enthalpy of 38 kcal/mol, consistent with the observed very slow disproportionation of **threo-4** only at elevated temperatures.

The TS structure of a second concerted [6+4]-ene pathway, **TS-erythro-4**, was not located on the PES. Attempts by scanning the C1–C1' and/or C5–H/C4'–H bonds (see [Figure 3](#) or [Figure 6](#) for the labeling) and using the highest energy structure in the scan as the initial structure for TS optimization lead to either the [4+2] cycloaddition TS structure **TS-exo-2** or the [4+2]-ene TS structure **TS-6**, both with lower energies than the initial structure. [Figure 6](#) illustrates the geometric similarity of the three structures; **TS-erythro-4** and **TS-exo-2** share the same forming C1–C1' bond while **TS-erythro-4** and **TS-6** share the

same C5–H···C4' H-transfer moiety. One might have even anticipated formation of an ambimodal transition state leading to several of these products.^{65,66,67,68,69,70,71} The existence of the two lower energy TS structures near **TS-erythro-4** on the PES likely makes **TS-erythro-4** no longer a stationary point. These calculations are consistent with the [6+4]-ene adduct **erythro-4** not being observed experimentally.

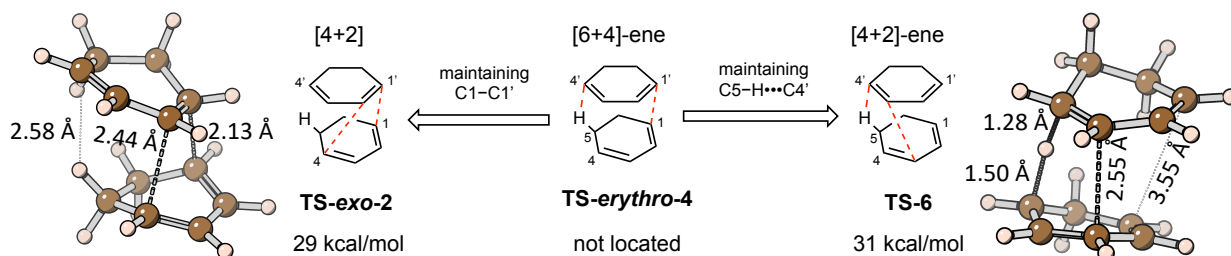


Figure 6. The structural relationship among three similar TS structures. ω B97XD/def2-TZVP enthalpies (ΔH_{298K}) of the optimized structures are shown.

Concerted [4+2]-ene pathways. As shown in [Figure 5](#), the computed enthalpic barriers of [4+2]-ene reactions are 2–11 kcal/mol higher than those of the [4+2] cycloaddition and [6+4]-ene pathways. A plausible reason for the higher energies of the [4+2]-ene TS structures is that the conjugation between the dienes in the bottom ring ([Figure 5](#)) is lost in the [4+2]-ene TS structures whereas it is remained in the TS structures of the [4+2]-cycloadditions and [6+4]-ene reaction. These >30 kcal/mol large barriers of the [4+2]-ene reactions are consistent with the fact that [4+2]-ene products are not observed experimentally.

Stepwise pathways. [Figure 7](#) shows the 1 atm enthalpic reaction profiles of the stepwise pathways. The initial C–C bond formation between two molecules of **1**, via the *rac* addition (the left branch) or the *meso* addition (the right branch), leads to a diradical intermediate **rac-8** or **meso-8**. **TS-meso** is computed to be 4 kcal/mol lower in enthalpy than **TS-rac**; **rac-8** and **meso-8** are computed to be similar in enthalpy. **rac-8** and **meso-8** have *anti* conformations around the forming C–C bonds. The search for stepwise TS structures in *gauche* conformations lead to concerted TS structures. For example, the two

gauche conformations of **TS-rac** evolved into **TS-endo-2** and **TS-threo-4** during TS optimization. It seems that only the *anti* conformations of the stepwise TS structures are stationary points on the PES at the ω B97XD/def2-TZVP level of theory. In the second step, two TS structures starting from **rac-8** (or **meso-8**) were located, affording [2+2]-cycloadduct **anti-3** (or **syn-3**) and [4+2]-cycloadduct **endo-2** (or **exo-2**). The [4+2] cycloadducts are computed to be about 8-11 kcal/mol more stable than the [2+2] cycloadducts.

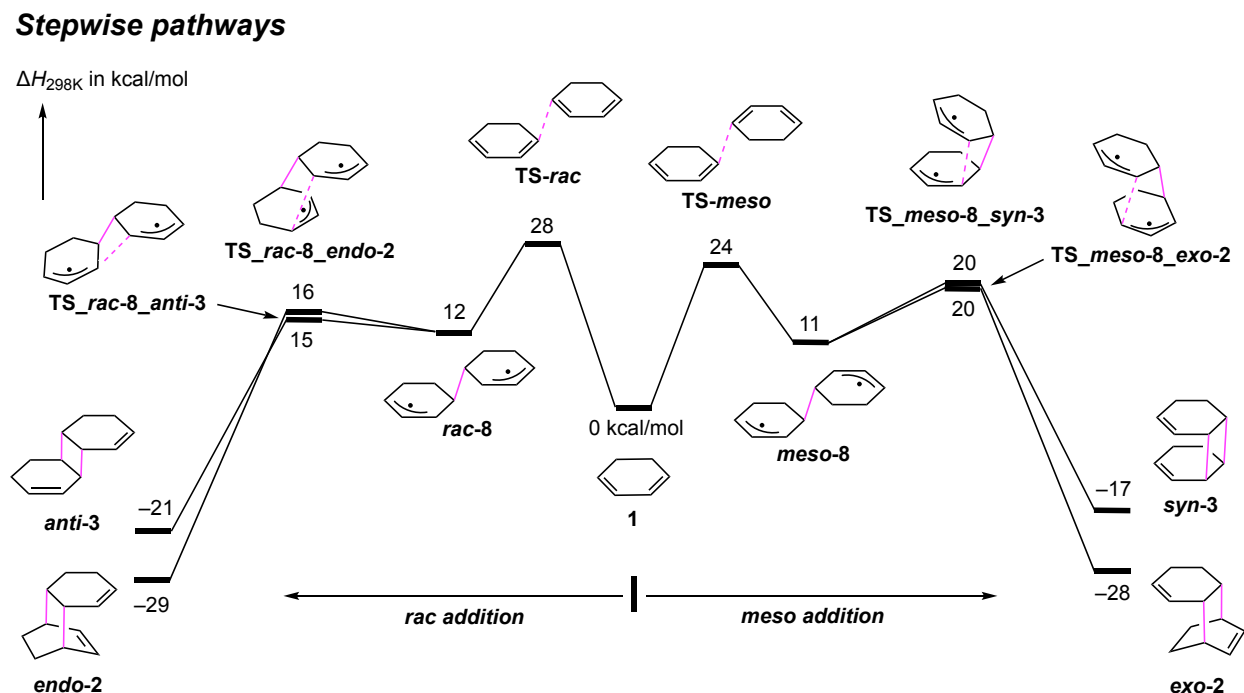


Figure 7. 1 atm enthalpic reaction profiles of stepwise pathways of 1,3-cyclohexadiene dimerization, calculated at the ω B97XD/def2-TZVP level of theory.

Formations of **exo-2** and **syn-3** share the same stepwise *meso* addition mechanism. Their respective TSs (**TS_meso-8_exo-2** and **TS_meso-8_syn-3**) for the second bond formation from the same intermediate **meso-8** were computed to have the same enthalpy of 20 kcal/mol. From the *anti* conformation of **meso-8**, more rotation about the first

formed C—C bond (~ 180 degrees, see [Figure 3](#)) is necessary in order to reach a geometry for the second bond to form to give **syn-3**. This might be the reason that **syn-3** has a lower product ratio than **exo-2** in experiment.

Many structures in the stepwise pathways are open-shell singlet states with significant multi-reference character. Single-reference DFT calculations using the broken-symmetry approach, which is what we used to compute the energies of, for example, **TS_meso** and **TS_rac** ([Table 1](#)), introduce spin contamination from the triplet to the open-shell singlet wave functions, as indicated by the $\langle S^2 \rangle$ values from broken-symmetry DFT calculations, for instance $\langle S^2 \rangle = 0.62$ for **TS_meso**. The spin-contamination can be removed by the Yamaguchi and Houk spin-projection procedure.⁵³

However, either the spin-contaminated or the spin-projected energies shows that the stepwise **TS_meso** is lower in energy than the concerted **TS_endo-2**, in contradiction to the experimental activation energies E_a in [Table 1](#). In order to compare the computed barriers of the stepwise pathways with the concerted pathways at a consistent level of theory, we resorted to NEVPT2 calculations. These NEVPT2 calculations are based on CASSCF(8,8) wavefunctions and, in addition to the fully-accounted dynamic electron correlation within the active space, the dynamic electron correlation outside of the active space is recovered through the 2nd order perturbation theory. As shown in [Table 1](#), **TS_meso** was computed to be 1 kcal/mol higher in enthalpy than **TS_endo-2** at the NEVPT2(8,8)/def2-TZVP//(U) ω B97XD/def2-TZVP level, consistent with the experimental E_a . However, the 3-5 kcal/mol difference between **TS_meso** and **TS_rac** at ω B97XD and NEVPT2 levels is larger than the experimental E_a , though this large difference is consistent with previous calculations.²⁸

The [4+2] cycloadducts **endo-2** and **exo-2** may be formed by either a concerted or stepwise mechanism as shown in [Figure 3](#). The NEVPT2 calculations in [Table 1](#) suggest that these two [4+2]-cycloadducts are formed by different mechanisms. For **endo-2**, the concerted mechanism is computed to be enthalpically more favorable whereas for **exo-2**, the stepwise mechanism is more favorable.

Although NEVPT2 calculations distinguishes the concerted and stepwise pathways reasonably well, they underestimate the enthalpic barriers of most pathways by about 4 kcal/mol, when compared against the experimental activation energy E_a (Table 1). We recommend referring to CCSD(T) barriers for the comparison with experimental E_a , and to the NEVPT2 barriers for comparing relative barrier heights, especially between the concerted and stepwise pathways. Irrespective of the level of theory, the concerted and stepwise pathways were computed to have enthalpic barriers within 5 kcal/mol. The small enthalpic difference between these TS structures are consistent with the experiment, confirming the competitive nature of the concerted and stepwise mechanisms in this reaction.

We summarize our calculations and discussions on the 1 atm PES of the thermal dimerization of cyclohexadiene as follows:

- For **endo-2**, the concerted [4+2] cycloaddition is computed to be more favorable than the stepwise mechanism at both the ω B97XD (spin-projected) and NEVPT2(8,8) levels. The CCSD(T) computed ΔH_{298K}^\ddagger for the concerted [4+2] cycloaddition gives the best agreement with the experimental E_a .
- For **exo-2**, the stepwise mechanism through the **meso-8** intermediate is supported against the concerted [4+2] cycloaddition by both the ω B97XD and NEVPT2(8,8) calculations.
- For **threo-4**, the concerted [6+4]-ene mechanism has the lowest ΔH_{298K}^\ddagger among all the reactions considered, as shown by the NEVPT2 and CCSD(T) calculations. The CCSD(T) ΔH_{298K}^\ddagger for this reaction is in excellent agreement with the experimental E_a .
- For **syn-3**, the thermally allowed stepwise mechanism through the **meso-8** intermediate is favored over the concerted mechanism by both the ω B97XD (spin-projected) and NEVPT2(8,8) calculations; however, both methods give an underestimation (5-6 kcal/mol) of the experimental activation energy.

- For *anti-3*, similar as *syn-3*, only the stepwise mechanism through the *rac-8* intermediate is thermally allowed. Only the NEVPT2(8,8) calculations give a reasonable estimation of the experimental activation energy.
- The above calculations are in good agreement with the previous calculations by Ess *et al.*²⁸ In addition, we explored the plausible [4+2]-ene mechanisms that were not considered before. The large computed barriers (> 31 kcal/mol at ω B97XD/def2-TZVP level of theory) are consistent with the fact that the corresponding [4+2]-ene products **5** and **6** were not observed experimentally.

Reaction profiles under pressure

Figure 8 shows the computed profiles of the effective energy ΔG_{tot} (see eq. 1) and cavity volume (the volume of the vdW cavity hosting the molecule in the continuum; see Computational Methodology for details) profiles of four different types of dimerization of 1,3-cyclohexadiene—the concerted [4+2]-cycloaddition, concerted [6+4]-ene reaction, concerted [4+2]-ene reaction, and the first step of a stepwise addition. For each type of reaction, one stereo version is shown and the others are given in the SI. For example, only the *endo* [4+2] cycloaddition is shown in Figure 8 and the *exo* cycloaddition is given in the SI. The profiles at 0 GPa are from the intrinsic reaction coordinate calculations; the high-pressure profiles are computed using the XP-PCM method based on the 0 GPa structures.

A first look shows that the four types of reaction have very different profiles, for example, in the location of the TS structure along the reaction coordinate and in the shape of the ΔG_{tot} and volume profiles. They do share a common feature—the ΔG_{tot} profile decreases as the pressure increases, which is consistent with the expected negative activation volumes of these dimerizations.

Concerted [4+2] cycloaddition. The concerted [4+2] cycloaddition has a fairly late TS at about 2/3 of the entire reaction course. The reaction profile is similar to other [4+2] cycloadditions previously studied using the same XP-PCM method.^{17,72,73} In the current

endo-cycloaddition, the first 1/4 of the PES is rather flat, where two isolated 1,3-cyclohexadiene molecules reorient themselves in a proper geometry for the cycloaddition and begin to approach one another; the latter motion would lead to a decrease of the separation between the molecules. At high pressure, a minimum of a vdW complex develops prior to the TS, as noted previously by us^{17,72} and by Loco et. al.⁵⁰ The minimum is very shallow at low pressures (may be difficult to see in the figure, but it is there) but becomes apparent at 5.7 GPa. This minimum also shifts towards the TS as the pressure increases. The emergence of a pre-TS minimum and the shift of it towards the TS could be explained by the pressure-enhanced vdW complex formation. The higher the pressure, the shorter the vdW separation between the molecules, and the smaller the volume of such complex. The favorable pV term of the enthalpy leads to the appearance of a minimum for the complex. This phenomenon of a pre-TS minimum seems to be common in bimolecular reactions; the other three reactions in [Figure 8](#) also exhibits such a feature, especially in the concerted [6+4]-ene reaction, where deep pre-TS minima at high pressures are suggested by the calculations.

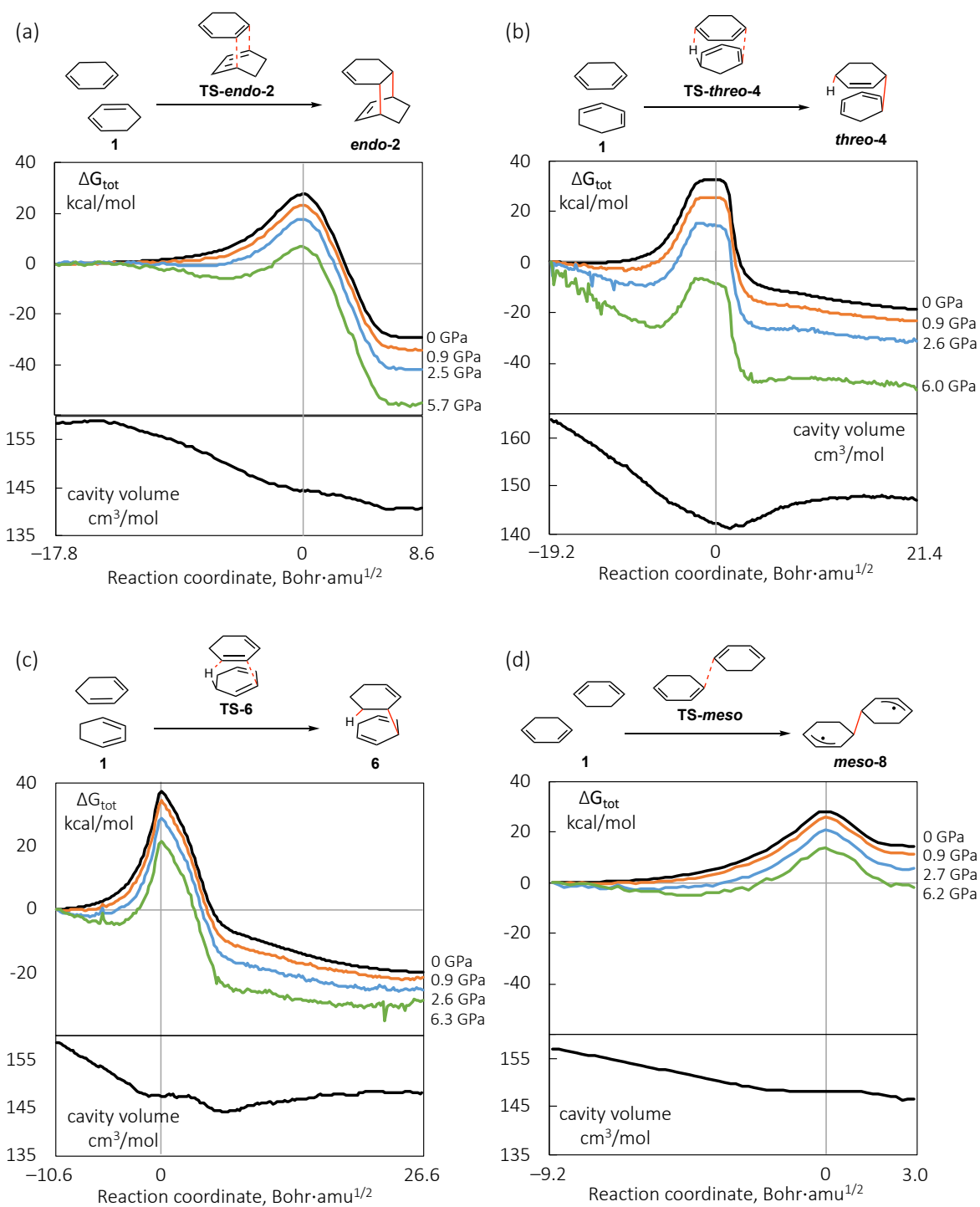


Figure 8. Effective reaction profiles (ΔG_{tot} in eq. 1) at different pressures and cavity volume profiles (vdW cavity with a scaling factor of 1.2 of the Bondi radii) of concerted [4+2] cycloaddition, concerted [6+4]-ene reaction, and the first step of the *meso* stepwise addition of cyclohexadiene dimerization, calculated by the XP-PCM method at the ω B97XD/def2-TZVP level.

The cavity volume profile of the *endo* [4+2] cycloaddition also shows a flat region at the beginning of the reaction; this is where the two molecules reorient themselves with a rotation before approaching each other. Afterwards, the cavity volume, as defined in the PCM model, decreases monotonically during the course of bond formation and does not change much when the bond formation is complete at the end of the profile. A nice correspondence between the cavity volume profile and the ΔG_{tot} profile is evident—at the beginning and end of the reaction, the volume and ΔG_{tot} profiles are both flat, whereas during the bond formation, the decreasing volume is matched by the enthalpy decrease at high pressures.

Concerted [6+4]-ene reaction. In the *threo* type [6+4]-ene reaction (Figure 8b), the concurrent C–C bond formation and H-transfer at the 1,4 positions of one ring and 1,5 positions of the other results in a substantial overlap of the two rings in the TS, more than that in the [4+2] cycloaddition TS. A top view (Figure 9) of this TS structure, **TS-*threo*-4**, shows that the two rings are almost coaxial and the CH/CH₂ groups are in a staggered conformation. On the contrary, the [4+2] cycloaddition TS has less overlap between the two rings as shown in the top view. The greater overlap of the rings in **TS-*threo*-4** leads to a more compact structure and a smaller volume of the structure, compared with **TS-*endo*-2**. The vdW cavity of **TS-*threo*-4** is 142 cm³/mol, compared with 145 cm³/mol for **TS-*endo*-2**. Note that 1 cm³/mol difference in volume corresponds to 0.24 kcal/mol difference in enthalpy at 1 GPa. The greater overlap of the rings and the highly-ordered staggered conformation in **TS-*threo*-4** is correlated with the small pre-exponential factor (i.e., small entropy of the TS) in the Arrhenius equation for the *threo* [6+4]-ene reaction (as discussed in the 1 atm PES section), compared with other reactions.

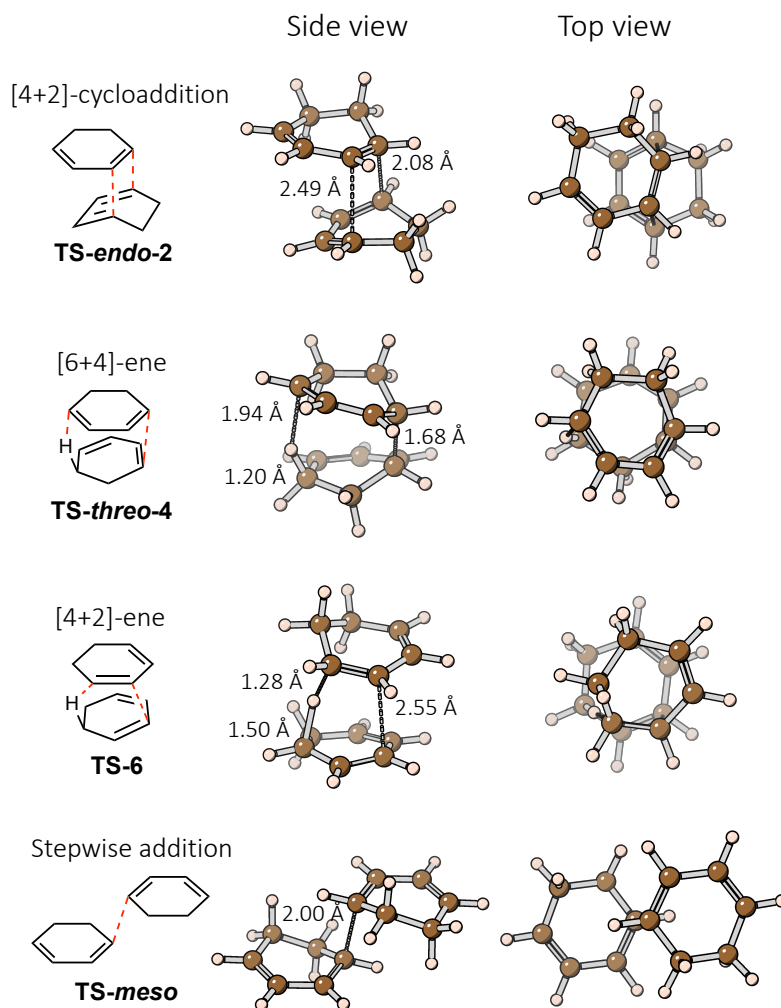


Figure 9. Two views of the ω B97XD/def2-TZVP optimized gas-phase TS structures with key bond distances shown.

The 0 GPa PES of the *threo* [6+4]-ene reaction has a rather flat region near the TS (Figure 8b), during which the C \cdots C and C \cdots H distances of the forming bonds (indicated by red dashes in **TS-threo-4**) change from 1.9 Å and 2.3 Å to 1.7 Å and 1.8 Å, respectively. After the flat region of the PES, the H-transfer completes in a few steps with a fast and substantial energy decrease. Then, a long and slow conformational change takes place in the last 1/3 of the reaction process. This conformational change mainly features the separation of the C, from which the H is transferred, from the newly formed C-H bond. Ignoring the last 1/3 of the profile of conformational change, this reaction also has a very

late TS. The cavity volume of the system decreases from the beginning of the reaction to about the point at which the H-transfer completes (i.e., a bit past the TS). Then the cavity increases, as the ene-adduct opens up to adapt to its optimal conformation at 0 GPa.

At high pressures, a pre-TS vdW complex minimum develops, similar to the case of the [4+2] cycloaddition. But this minimum in the [6+4]-ene reaction is much deeper compared with that in the [4+2] cycloaddition. A most likely reason is that the separated reactant molecules occupy a larger volume (164 cm³/mol) than in the [4+2] cycloaddition (158 cm³/mol), so that a greater volume reduction is possible in forming the vdW complex. The flat TS region of the PES at 0 GPa becomes tilted with the post-TS region lowering in enthalpy at high pressures, due to the monotonical volume decrease in this region. A clear shift of the TS towards the reactant is seen at high-pressures. The shift of TS at high pressure is consistent with the Hammond postulate⁷⁴ that the TS shifts towards the reactant when the reaction becomes more exothermic. However, note that the TS shift is apparent only in the [6+4]-ene reaction, not so in the other three reactions in [Figure 8](#), though all these reactions become more exothermic (or less endothermic) at high pressures. One distinct feature of the [6+4]-ene reaction is that the cavity volume decreases in the TS region, while in the other three reactions, the cavity volume stays almost constant in the TS region. Therefore, the effect of pressure is larger on the PES in the TS region in the [6+4]-ene reaction, leading to an apparent shift of the TS towards the reactant. The shift of TS along reaction coordinate under pressure has been noted previously.^{17,40,48,49}

Concerted [4+2]-ene reaction. In contrast to the flat TS region in the [6+4]-ene reaction, the [4+2]-ene reaction has a sharp maximum in the TS region ([Figure 8c](#)). We inspected the TS structures in the two reactions to understand the reason. In the [6+4]-ene **TS-threo-4**, the C–C bond is almost fully formed at a distance of 1.68 Å while the H is barely transferred with distances of 1.20 and 1.90 Å for the breaking and forming C–H bonds ([Figure 9](#)). On the contrary, in the [4+2]-ene **TS-6**, the H-transfer is substantial with 1.50 and 1.28 Å for the two C–H bonds but the C–C bond to be formed is at a large distance of 2.55 Å. The shapes of PESs near the TSs and the structural features of the TSs in these two ene reactions suggest that the H-transfer is associated with a much larger energy change than the C–C bond formation. When the TS structure of the ene reaction is dominated by C–

C bond formation, the PES near the TS is flat, as in the [6+4]-ene reaction; when the TS structure is governed by H-transfer, the PES near the TS is sharp, as in the [4+2]-ene reaction.

The [4+2]-ene reaction also has a long course of conformational change in the second half of the profile. Again, this is due to the opening up of the molecule after the H-transfer. Correspondingly, the volume increases during the course of this conformational change (Figure 8c). Interestingly, the volume profile has a flat region near the TS; the reason is two-fold. In the region before the TS, where H-transfer starts to take place, the C...C distance in the C-H...C moiety stays almost constant (at about 2.8 Å), so does the distance of the C-C bond to be formed (at about 2.6 Å). During this course, there is little movement of the two molecules against each other, which leads to little volume change. In the region after the TS, the C-C bond starts to form, which reduces the separation between the two rings and should lead to volume reduction. However, this effect is counter-balanced by the opening-up of the C...H-C moiety after H-transfer that results in a volume increase. The overall effect is that the volume stays constant in quite a region after the TS. Afterwards, the C-C bond formation dominates for a short duration with a decrease of the cavity volume, before the final conformational change takes over and leads to a slow volume increase.

The cavity volume of the [4+2]-ene **TS-6** is 147 cm³/mol, larger than those of the **TS-endo-2** in the [4+2]-cycloaddition (145 cm³/mol) and **TS-threo-4** in the [6+4]-ene reaction (142 cm³/mol). Consequently, the lowering of the enthalpy at high pressure is much less in the [4+2]-ene TS than in the other two reactions. As discussed above, because the cavity volume does not change in the TS region in the [4+2]-ene reaction, one would not expect a shift the TS location under pressure (Figure 8c).

Stepwise addition. Moving on to the stepwise mechanism, Figure 8d shows the reaction profiles of the *meso* addition. Compared with the above-discussed concerted reactions, this *meso* addition has a rather short course, especially in the post-TS region. The C-C distance of the formed bond changes from 2.00 Å in **TS-meso** to 1.57 Å in the adduct **meso-8**. The cavity volume of the system decreases in the *meso*-addition, but with a much

less volume reduction compared with the above concerted reactions where two bonds are formed. Consequently, pressure provides much less reduction of the reaction barrier for the *meso* addition. The *meso*-adduct **meso-8** is calculated to be higher in enthalpy than the reactants at pressures lower than 6.2 GPa.

Calculations of activation volumes

In addition to activation energy, activation volume also provides information about the transition state, arguably, in a more tangible manner. The volume/size of a TS structure is directly related to its geometry. While competing mechanisms of a reaction can sometimes be difficult to distinguish based on activation energies, they may be distinguishable by activation volumes when the competing TS structures have very different geometries. This is especially useful in studying the stepwise vs concerted mechanisms of cycloadditions, given that the stepwise mechanism often has a less negative activation volume.^{24,25}

In order to calculate the activation volume of a reaction, the barriers computed by XP-PCM are plotted against the pressure (Figure 10). The $\Delta G_{tot}^\ddagger(p)$ data shows a nice linear relationship. The slope of the fitted line gives the activation volume, according to eq. (2). Note that the free energy $\Delta G_{tot}^\ddagger(p)$ does not contain zero-point vibrational correction and thermal correction, assuming their negligible contributions to ΔV^\ddagger . The components of ΔG^\ddagger are the electronic energy and cavitation energy computed by XP-PCM (eq. 1). Note that for the ΔV^\ddagger calculations, ΔG_{tot}^\ddagger at different pressures are computed using as the reference isolated reactant molecules, not the vdW complexes (pre-TS minima) in Figure 8. This is to ensure a common reference (isolated reactants) in the ΔV^\ddagger comparison for different mechanisms.

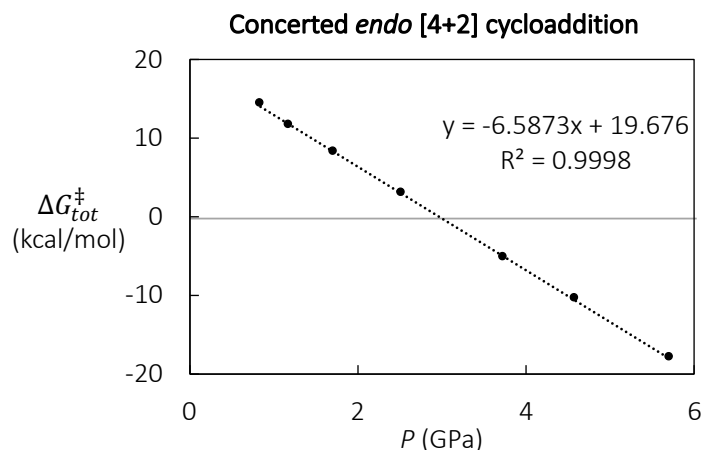


Figure 10. The plot of computed activation energies at different pressures $\Delta G_{tot}^{\ddagger}(p)$ in the concerted *endo* [4+2]-cycloaddition, for computing activation volume ΔV^{\ddagger} .

Table 2 shows the computed activation volumes ΔV^{\ddagger} from linear fitting of the computed $\Delta G_{tot}^{\ddagger}$ at different pressures, which are compared with experimental values.

The computed ΔV^{\ddagger} are -27.7 and -28.2 cm^3/mol for the concerted *endo* and *exo* [4+2] cycloadditions. Less negative ΔV^{\ddagger} of -20.5 and -21.4 cm^3/mol are computed for the stepwise mechanisms that may also deliver the two [4+2] cycloadducts. Comparison with experimental ΔV^{\ddagger} highly suggests that the *endo* [4+2] cycloaddition follows a concerted mechanism, but the *exo* adduct is formed through a stepwise mechanism.

The concerted [6+4]-ene reaction is computed to have the most negative ΔV^{\ddagger} of -32.1 cm^3/mol , in excellent with the experimental value, thus conforming the concerted mechanism of this reaction. This large negative ΔV^{\ddagger} for the [6+4]-ene reaction is consistent with the compact geometry of the TS structures, as discussed in the reaction profile under pressure section.

For the [2+2]-cycloadduct **syn-3**, the computed ΔV^{\ddagger} of the stepwise mechanism through the **meso-8** intermediate is in excellent agreement with the corresponding experimental data. For **anti-3**. The computed ΔV^{\ddagger} of the stepwise mechanism through the **rac-8** intermediate is in good agreement with the experimental data with a slight

overestimation. These calculations support the stepwise mechanisms for the [2+2] cycloadditions.

Table 2. Calculated (ω B97XD/def2-TZVP) and experimental activation volumes ΔV^\ddagger .

Reaction product	computed ΔV^\ddagger (cm ³ /mol)	experimental ΔV^\ddagger (cm ³ /mol)
endo-2 [4+2]-cycloadduct	-27.7 (concerted)	-28
	-20.5 (stepwise via TS-rac)	
exo-2 [4+2]-cycloadduct	-28.2 (concerted)	-22
	-21.4 (stepwise via TS-meso)	
threo-4 [6+4]-ene adduct	-32.1 (concerted)	-32
syn-3 [2+2]-cycloadduct	-21.4 (stepwise via TS-meso)	-22
anti-3 [2+2]-cycloadduct	-20.5 (stepwise via TS-rac)	-18

Summary and Conclusions

This work is part of our continuing efforts to apply a new quantum chemical method, the extreme pressure polarizable continuum model (XP-PCM), to the study of reaction energy profiles under pressure, and to calculate activation volumes. The method has been tutorially reviewed and applied by the present authors and Hoffmann¹⁷ in 2017 to a set of pericyclic reactions where interesting phenomena on reaction energy profiles under pressure were revealed by calculations, such as the shift of the transition state, changes in the rate-determining step, *etc.* In addition, a reasonable agreement of the computed activation volumes with the experimental values was discovered. The evolution of the van der Waals volume of the reactive system upon proceeding from the reactants to products, as a chemical relevant diagnostic to analyze the effect of the pressure on the reaction energy profile, was emphasized.

In this work, the XP-PCM computational method is applied to the study of the pressure effects on the competing mechanisms of the thermal dimerization of the 1,3-

cyclohexadiene, providing, for the first time, accurate calculations of activation volumes, compared with the experimental ones. The activation volumes are of primary relevance for the determination of the competing mechanisms in this reaction.

The thermal dimerization of 1,3-cyclohexadiene has been studied experimentally in solution and at various conditions of temperature and pressure, by Klärner *et al.*²⁶ in 1986 and computationally by Ess *et al.*²⁸ in 2008 in the gas phase (1 atm). In experiment, the observed products were from symmetry allowed [4+2] cycloadditions (***endo-2***, ***exo-2***), [6+4] ene reaction (***threo-4***) and symmetry-forbidden [2+2] cycloadditions (***syn-3***, ***anti-3***). While the thermal [2+2] cycloadditions are usually expected to be formed via a stepwise mechanism, all the other products can be formed through competing, concerted or stepwise mechanisms. Based on a simple interpretation of the experimental activation volume (all negative) and of the activation energy, Klärner *et al.* heuristically suggested that the dimerizations to ***endo-2*** and ***threo-4*** follow a concerted mechanism, while the reaction affording ***exo-2*** follows a stepwise mechanism that is in common with the mechanism leading to the ***syn-3*** [2+2]-adduct. The 2008 computational study of the dimerization of the 1,3-cyclohexadiene focused on the activation energies; the reaction barriers for the competing concerted and stepwise mechanism were computed to be within a range of 5 kcal/mol, confirming the competitive nature between these mechanisms, but with slight differences from the experiment in what concerns the order of the activation energies.

With respect to the previous computational study by Ess *et al.*, we have first expanded the exploration of the reaction energy profile of various mechanisms of the dimerization of the 1,3-cyclohexadiene in the gas phase, in searching for both a more accurate evaluation of the activation energies and a [4+2]-ene mechanism not considered previously. Then, we have applied the XP-PCM method to study the effect of the pressure on the reaction energy profile and to compute the activation volumes.

The gas-phase transition structure for the various concerted and stepwise mechanisms have been evaluated at the ω B97XD/def2-TZVP level and the corresponding activation energies computed at the NEVPT2(8,8)/def2-TZVP level, and the CCSD(T)/def2-

TZVP level for the concerted only mechanisms. The comparison between the NEVPT2(8,8) activation energies in the concerted and stepwise mechanism and the experimental data gives support that products **endo-2** and **threo-4** follow a concerted mechanism, while the product **exo-2** follow a stepwise mechanism in common with the mechanism leading to the **syn-3** adduct, with an almost correct order in agreement with the experimental data. The CCSD(T) give the most accurate activation energies for the *endo* [4+2] cycloaddition and the [6+4]-ene reaction. For the [4+2]-ene mechanism not considered in the Ess et al. computational study, we have obtained the highest activation energies, consistently with the fact that the related products (**5** and **6**) were not observed experimentally.

The effect of the pressure on the energy profile has been evaluated using the XP-PCM method along with the gas phase intrinsic reaction path (at ω B97XD/def2-TZVP level) of the concerted **endo-2** [4+2] cycloaddition, the concerted [6+4]-ene and [4+2]-ene reactions and for the first step of the stepwise mechanism leading to the **exo-2** and **syn-3** adducts. The effect of the pressure on the energy profile has been correlated with the profile of the volume of the van der Waals cavity enclosing the reacting systems. The energy profiles of these four types of reactions share a common feature: the energy profile decreases as the pressure increases, consistent with the expected negative activation volumes of these dimerizations. Furthermore, they are characterized by the emergence of a pre-TS minimum, corresponding to a van der Waals complex, and the shift of it toward the transition state, a feature that can be explained by the smaller volume of such complex with respect to the separated reactant and by the corresponding favorable (i.e. negative) enthalpic pV term to the energy profile. Except for the concerted [6+4]-ene reaction, all other reactions do not present, in the range of pressure (1-6 GPa) explored, a significant shift of the location of the transition state along the reaction coordinate. The shift at high pressure of the transition state of the concerted [6+4]-ene reaction is consistent with the Hammond postulate that the TS shifts towards the reactant when the reaction is more exothermic. Furthermore, it may be related to the fact that concerted [6+4]-ene reaction features a decrease of the vdW cavity volume of the reactant systems in the TS region while in the other reactions, the vdW cavity volume stays almost constant.

The activation volumes have been computed as the derivative with respect to the pressure of the activation energy extracted from the energy profiles of the various possible mechanism as a function of the pressure for all the five observed adducts, for which the experimental data are available. The comparison between the computed activation volume for the alternative mechanism and experimental data shows in a very clear way that the products **endo-2** and **threo-4** are compatible only with a concerted mechanism, while the product **exo-2** is compatible only with a stepwise mechanism in common with the **syn-3** product. Also the computed activation volume for the stepwise mechanism for the **anti-3** product is in good agreement with the experimental data.

As in the case of dimerization of the 1,3-cyclohexadiene the experimental activation volumes (and not the activation energies) have been the primary basis for the heuristic suggestion of the mechanisms in operation for this reaction, we may consider the agreement between the computed and experimental activation volumes a more direct validation of the suggested mechanisms.

Acknowledgement

We thank Roald Hoffmann and Frank Klärner for helpful discussions. R.C. thanks the support of the framework of the COMP-HUB Initiative of the Department of Chemistry, Life Sciences and Environmental Sustainability of the University of Parma, as part of the 'Departments of Excellence' program of the Italian Ministry for Education, University and Research (MIUR, 2018-2022).

Supporting Information

- 3D drawings of transition state structures, a more detailed description of the XP-PCM method, PES of the disproportionation of **threo-4**, and supplementary reaction profiles to [Figure 8](#) (PDF).

- Raw output files of calculations containing optimized geometries and absolute energies (ZIP).

References

¹ Arrhenius, S. Über Die Dissociationswärme Und Den Einfluss Der Temperatur Auf Den Dissociationsgrad Der Elektrolyte. *Zeitschrift Für Physikalische Chemie* **1889**, *4U* (1), 96–116. <https://doi.org/10.1515/zpch-1889-0408>.

² Arrhenius, S. Über Die Reaktionsgeschwindigkeit Bei Der Inversion von Rohrzucker Durch Säuren. *Zeitschrift Für Physikalische Chemie* **1889**, *4* (1). <https://doi.org/10.1515/zpch-1889-0116>.

³ Bell, R. P. The Tunnel Effect in Chemistry. **1980**. <https://doi.org/10.1007/978-1-4899-2891-7>.

⁴ Glasstone, S.; Laidler, K. J.; Eyring, H. *The Theory of Rate Processes: The Kinetics of Chemical Reactions, Viscosity, Diffusion and Electrochemical Phenomena*; McGraw-Hill Book Company: New York, 1941.

⁵ Noble, W. J. L. Kinetics of Reactions in Solutions Under Pressure; Progress in Physical Organic Chemistry; John Wiley & Sons, Inc., 1967; Vol. 5, pp 207–330. <https://doi.org/10.1002/9780470171844.ch3>.

⁶ Asano, T.; Noble, W. J. L. Activation and Reaction Volumes in Solution. *Chem Rev* **1978**, *78* (4), 407–489. <https://doi.org/10.1021/cr60314a004>.

⁷ Eldik, R. V.; Asano, T.; Noble, W. J. L. Activation and Reaction Volumes in Solution. 2. *Chem Rev* **1989**, *89* (3), 549–688. <https://doi.org/10.1021/cr00093a005>.

⁸ Drljaca, A.; Hubbard, C. D.; Eldik, R. van; Asano, T.; Basilevsky, M. V.; Noble, W. J. le. Activation and Reaction Volumes in Solution. 3. *Chem Rev* **1998**, *98* (6), 2167–2290. <https://doi.org/10.1021/cr970461b>.

-
- ⁹ Basilevsky, M. V.; Weinberg, N. N.; Zhulin, V. M. Pressure Dependence of Activation and Reaction Volumes. *J Chem Soc Faraday Transactions 1 Phys Chem Condens Phases* **1985**, *81* (4), 875–884. <https://doi.org/10.1039/f19858100875>.
- ¹⁰ Basilevskii, M. V.; Ryaboi, V. M.; Weinberg, N. N. Nonequilibrium Effects in Kinetics of Cycloaddition Reactions under High Pressure. *J Phys Chem* **1991**, *95* (14), 5533–5540. <https://doi.org/10.1021/j100167a032>.
- ¹¹ Basilevsky, M. V.; Weinberg, N. N. A Microscopic Theory of Chemical Reactions under High Pressures. *Can J Phys* **1995**, *73* (5–6), 267–272. <https://doi.org/10.1139/p95-038>.
- ¹² Jenner, G. High Pressure Kinetic Investigations in Organic and Macromolecular Chemistry. *Angewandte Chemie International Edition in English* **1975**, *14* (3), 137–143. <https://doi.org/10.1002/anie.197501371>.
- ¹³ Jenner, G. High Pressure Chemistry, Biochemistry and Materials Science. In *High Pressure Kinetic Effects as Mechanistic Probes in Organic Chemistry*; Winter, R., Jonas, J., Eds.; NATO ASI Series (Series C: Mathematical and Physical Sciences); Springer: Dordrecht, 1993; Vol. 401, pp 345–366. https://doi.org/10.1007/978-94-011-1699-2_18.
- ¹⁴ Jenner, G. Activation of Organic Reactions. High Pressure vs New Emerging Activation Modes; High Pressure Molecular Science; Springer Netherlands, 1999; pp 313–330. https://doi.org/10.1007/978-94-011-4669-2_18.
- ¹⁵ Wurche, F.; Klärner, F.-G. The Effect of Pressure on Organic Reactions: Basic Principles and Mechanistic Applications; High Pressure Chemistry; Wiley-VCH Verlag GmbH, 2002; pp 41–96. <https://doi.org/10.1002/9783527612628.ch02>.
- ¹⁶ Hugelshofer, C.; Magauer, T. High-Pressure Transformations in Natural Product Synthesis. *Synthesis* **2014**, *46* (10), 1279–1296. <https://doi.org/10.1055/s-0033-1341073>.
- ¹⁷ Chen, B.; Hoffmann, R.; Cammi, R. The Effect of Pressure on Organic Reactions in Fluids—a New Theoretical Perspective. *Angewandte Chemie International Edition in English* **2017**, *56* (37), 11126–11142. <https://doi.org/10.1002/anie.201705427>.
- ¹⁸ Margetic, D. *High Pressure Organic Synthesis*; De Gruyter: Berlin, Boston, 2019. <https://doi.org/10.1515/9783110556841>.
- ¹⁹ Steinfeld, J. I.; Francisco, J. S.; Hase, W. L. *Chemical Kinetics and Dynamics*; Upper Saddle River, N.J. : Prentice Hall, 1999. (see Eq. 10.54);

-
- ²⁰ IUPAC. Compendium of Chemical Terminology, 2nd ed. (the "Gold Book"). Compiled by A. D. McNaught and A. Wilkinson. Blackwell Scientific Publications, Oxford (1997). Online version (2019-) created by S. J. Chalk. ISBN 0-9678550-9-8. <https://doi.org/10.1351/goldbook>.
- ²¹ Eyring, H.; Lin, S. H.; Lin, S. M. *Basic Chemical Kinetics*; Wiley: New York, 1980. pp.422-426.
- ²² Laidler, K. J. *Chemical Kinetics, 3rd Edition*; Pearson, 1987.
- ²³ Mozurkewich, M.; Benson, S. W. Negative Activation Energies and Curved Arrhenius Plots. 1. Theory of Reactions over Potential Wells. *J Phys Chem* **1984**, *88* (25), 6429–6435. <https://doi.org/10.1021/j150669a073>.
- ²⁴ Eckert, C. A.; Grieger, R. A. Mechanistic Evidence for the Diels-Alder Reaction from High-Pressure Kinetics. *J Am Chem Soc* **1970**, *92* (24), 7149–7153. <https://doi.org/10.1021/ja00727a021>.
- ²⁵ Klaerner, F.-G.; Krawczyk, B.; Ruster, V.; Deiters, U. K. Evidence for Pericyclic and Stepwise Processes in the Cyclodimerization of Chloroprene and 1,3-Butadiene from Pressure Dependence and Stereochemistry. Experimental and Theoretical Volumes of Activation and Reaction. *J Am Chem Soc* **1994**, *116* (17), 7646–7657. <https://doi.org/10.1021/ja00096a023>.
- ²⁶ Klärner, F.; Dogan, B. M. J.; Ermer, O.; Doering, W. von E.; Cohen, M. P. Mechanism of the Thermal 1,3-Cyclohexadiene Dimerization: A Non-Concerted Diels-Alder Reaction Leading to the Exo-[4+2] Adduct and a Novel [6+4]-Ene Reaction. *Angewandte Chemie Int Ed Engl* **1986**, *25* (1), 108–110. <https://doi.org/10.1002/anie.198601081>.
- ²⁷ Woodward, R. B.; Hoffmann, R. The Conservation of Orbital Symmetry. *Angewandte Chemie International Edition in English* **1969**, *8* (11), 781–853. <https://doi.org/10.1002/anie.196907811>.
- ²⁸ Ess, D. H.; Hayden, A. E.; Klärner, F.-G.; Houk, K. N. Transition States for the Dimerization of 1,3-Cyclohexadiene: A DFT, CASPT2, and CBS-QB3 Quantum Mechanical Investigation. *J Org Chem* **2008**, *73* (19), 7586–7592. <https://doi.org/10.1021/jo8011804>.
- ²⁹ Klärner, F.-G.; Wurche, F. The Effect of Pressure on Organic Reactions. *Journal für praktische Chemie* **2000**, *342* (7), 609–636. [https://doi.org/10.1002/1521-3897\(200009\)342:7<609::aid-prac609>3.3.co;2-q](https://doi.org/10.1002/1521-3897(200009)342:7<609::aid-prac609>3.3.co;2-q).

-
- ³⁰ Cammi, R. A New Extension of the Polarizable Continuum Model: Toward a Quantum Chemical Description of Chemical Reactions at Extreme High Pressure. *J Comput Chem* **2015**, *36* (30), 2246–2259. <https://doi.org/10.1002/jcc.24206>.
- ³¹ Stewart, S. G.; Harfoot, G. J.; McRae, K. J.; Teng, Y.; Yu, L.-J.; Chen, B.; Cammi, R.; Coote, M. L.; Banwell, M. G.; Willis, A. C. High-Pressure-Promoted and Facially Selective Diels-Alder Reactions of Enzymatically Derived Cis-1,2-Dihydrocatechols and Their Acetonide Derivatives: Enantiodivergent Routes to Homochiral and Polyfunctionalized Bicyclo[2.2.2]Octenes. *The Journal of Organic Chemistry* **2020**, *85* (20), 13080–13095. <https://doi.org/10.1021/acs.joc.0c01767>.
- ³² Fukuda, R.; Nakatani, K. Quantum Chemical Study on the High-Pressure Effect for [4 + 4] Retrocycloaddition of Anthracene Cyclophane Photodimer. *J Phys Chem C* **2019**, *123* (7), 4493–4501. <https://doi.org/10.1021/acs.jpcc.8b10825>.
- ³³ Pagliai, M.; Cammi, R.; Cardini, G.; Schettino, V. XP-PCM Calculations of High Pressure Structural and Vibrational Properties of P 4 S 3. *J Phys Chem* **2016**, *120* (27), 5136–5144. <https://doi.org/10.1021/acs.jpca.6b00590>.
- ³⁴ Caratelli, C.; Cammi, R.; Chelli, R.; Pagliai, M.; Cardini, G.; Schettino, V. Insights on the Realgar Crystal Under Pressure from XP-PCM and Periodic Model Calculations. *J Phys Chem* **2017**, *121* (46), 8825–8834. <https://doi.org/10.1021/acs.jpca.7b08868>.
- ³⁵ Cammi, R. Linear Chains of Hydrogen Molecules under Pressure: An Extreme-Pressure Continuum Model Study. *J Chem Phys* **2019**, *150* (16), 164122. <https://doi.org/10.1063/1.5075511>.
- ³⁶ Cammi, R.; Cappelli, C.; Mennucci, B.; Tomasi, J. Calculation and Analysis of the Harmonic Vibrational Frequencies in Molecules at Extreme Pressure: Methodology and Diborane as a Test Case. *J Chem Phys* **2012**, *137* (15), 154112. <https://doi.org/10.1063/1.4757285>.
- ³⁷ Pagliai, M.; Cardini, G.; Cammi, R. Vibrational Frequencies of Fullerenes C60 and C70 under Pressure Studied with a Quantum Chemical Model Including Spatial Confinement Effects. *J Phys Chem* **2014**, *118* (27), 5098–5111. <https://doi.org/10.1021/jp504173k>.
- ³⁸ Boccalini, M.; Cammi, R.; Pagliai, M.; Cardini, G.; Schettino, V. Toward an Understanding of the Pressure Effect on the Intramolecular Vibrational Frequencies of Sulfur Hexafluoride. *J Phys Chem* **2021**, *125* (29), 6362–6373. <https://doi.org/10.1021/acs.jpca.1c02595>.
- ³⁹ Fukuda, R.; Ehara, M.; Cammi, R. Modeling Molecular Systems at Extreme Pressure by an Extension of the Polarizable Continuum Model (PCM) Based on the Symmetry-Adapted

Cluster-Configuration Interaction (SAC-CI) Method: Confined Electronic Excited States of Furan as a Test Case. *J Chem Theory Comput* **2015**, *11* (5), 2063–2076.
<https://doi.org/10.1021/ct5011517>.

⁴⁰ Jha, S. K.; Brown, K.; Todde, G.; Subramanian, G. A Mechanochemical Study of the Effects of Compression on a Diels-Alder Reaction. *J Chem Phys* **2016**, *145* (7), 074307.
<https://doi.org/10.1063/1.4960955>.

⁴¹ Stauch, T. A Mechanochemical Model for the Simulation of Molecules and Molecular Crystals under Hydrostatic Pressure. *J Chem Phys* **2020**, *153* (13), 134503.
<https://doi.org/10.1063/5.0024671>.

⁴² Stauch, T. Quantum Chemical Modeling of Molecules under Pressure. *International Journal of Quantum Chemistry* **2021**, *121* (3), e26208. <https://doi.org/10.1002/qua.26208>.

⁴³ Boscoboinik, A.; Olson, D.; Adams, H.; Hopper, N.; Tysoe, W. T. Measuring and Modelling Mechanochemical Reaction Kinetics. *Chem Commun* **2020**, *56* (56), 7730–7733.
<https://doi.org/10.1039/d0cc02992k>.

⁴⁴ Scheurer, M.; Dreuw, A.; Epifanovsky, E.; Head-Gordon, M.; Stauch, T. Modeling Molecules under Pressure with Gaussian Potentials. *Journal of Chemical Theory and Computation* **2021**, *17* (1), 583–597. <https://doi.org/10.1021/acs.jctc.0c01212>.

⁴⁵ Deglint, E.; Martens, H.; Edwards, E.; Boon, N.; Dance, P.; Weinberg, N. Molecular Dynamics Calculation of Activation Volumes. *Phys Chem Chem Phys* **2010**, *13* (2), 438–440.
<https://doi.org/10.1039/c0cp01570a>.

⁴⁶ Spooner, J.; Wiebe, H.; Boon, N.; Deglint, E.; Edwards, E.; Yanciw, B.; Patton, B.; Thiele, L.; Dance, P.; Weinberg, N. Molecular Dynamics Calculation of Molecular Volumes and Volumes of Activation. *Phys Chem Chem Phys* **2012**, *14* (7), 2264–2277.
<https://doi.org/10.1039/c2cp22949h>.

⁴⁷ Spooner, J.; Yanciw, B.; Wiebe, B.; Weinberg, N. Reaction Profiles and Energy Surfaces of Compressed Species. *J Phys Chem* **2014**, *118* (4), 765–777.
<https://doi.org/10.1021/jp410496t>.

⁴⁸ Spooner, J.; Smith, B.; Weinberg, N. Effect of High Pressure on the Topography of Potential Energy Surfaces. *Can J Chem* **2016**, *94* (12), 1057–1064.
<https://doi.org/10.1139/cjc-2016-0295>.

-
- ⁴⁹ Plotnikov, N. V.; Martinez, T. J. Molecular Origin of Mechanical Sensitivity of the Reaction Rate in Anthracene Cyclophane Isomerization Reveals Structural Motifs for Rational Design of Mechanophores. *J Phys Chem C* **2016**, *120* (32), 17898–17908. <https://doi.org/10.1021/acs.jpcc.6b04924>.
- ⁵⁰ Loco, D.; Spezia, R.; Cartier, F.; Chataigner, I.; Piquemal, J.-P. Solvation Effects Drive the Selectivity in Diels–Alder Reaction under Hyperbaric Conditions. *Chem Commun* **2020**, *56* (49), 6632–6635. <https://doi.org/10.1039/d0cc01938k>.
- ⁵¹ Chai, J.-D.; Head-Gordon, M. Long-range corrected hybrid density functionals with damped atom-atom dispersion corrections. *Physical Chemistry Chemical Physics* **2008**, *10* (44), 6615–6620 DOI: 10.1039/b810189b.
- ⁵² Weigend, F.; Ahlrichs, R. Balanced basis sets of split valence, triple zeta valence and quadruple zeta valence quality for H to Rn: Design and assessment of accuracy. *Physical Chemistry Chemical Physics* **2005**, *7* (18), 3297–3305 DOI: 10.1039/b508541a.
- ⁵³ Yamaguchi, K.; Takahara, Y.; Fueno, T.; Houk, K. N. Extended Hartree-Fock (EHF) Theory of Chemical Reactions. *Theor Chim Acta* **1988**, *73* (5–6), 337–364. <https://doi.org/10.1007/bf00527740>.
- ⁵⁴ Angeli, C.; Cimiraglia, R.; Evangelisti, S.; Leininger, T.; Malrieu, J.-P. *J. Chem. Phys.*, **2001**, *114*, 10252.
- ⁵⁵ Angeli, C.; Cimiraglia, R.; Malrieu, J.-P. *Chem. Phys. Lett.*, **2001**, *350*, 297.
- ⁵⁶ Angeli, C.; Cimiraglia, R.; Malrieu, J.-P. *J. Chem. Phys.*, **2002**, *117*, 9138.
- ⁵⁷ Purvis, G. D., III; Bartlett, R. J. A full coupled-cluster singles and doubles model: The inclusion of disconnected triples. *J. Chem. Phys.* **1982**, *76* (4), 1910–1918 DOI: 10.1063/1.443164.
- ⁵⁸ Pople, J. A.; Head-Gordon, M.; Raghavachari, K. Quadratic configuration interaction. A general technique for determining electron correlation energies. *J. Chem. Phys.* **1987**, *87* (1), 5968–5975 DOI: 10.1063/1.453520.
- ⁵⁹ Frisch, M. J.; Trucks, G. W.; Schlegel, H. B.; Scuseria, G. E.; Robb, M. A.; Cheeseman, J. R.; Scalmani, G.; Barone, V.; Petersson, G. A.; Nakatsuji, H.; Li, X.; Caricato, M.; Marenich, A. V.; Bloino, J.; Janesko, B. G.; Gomperts, R.; Mennucci, B.; Hratchian, H. P.; Ortiz, J. V.; Izmaylov, A. F.; Sonnenberg, J. L.; Williams-Young, D.; Ding, F.; Lipparini, F.; Egidi, F.; Goings, J.; Peng, B.; Petrone, A.; Henderson, T.; Ranasinghe, D.; Zakrzewski, V. G.; Gao, J.; Rega, N.; Zheng, G.;

Liang, W.; Hada, M.; Ehara, M.; Toyota, K.; Fukuda, R.; Hasegawa, J.; Ishida, M.; Nakajima, T.; Honda, Y.; Kitao, O.; Nakai, H.; Vreven, T.; Throssell, K.; Montgomery, Jr., J. A.; Peralta, J. E.; Ogliaro, F.; Bearpark, M. J.; Heyd, J. J.; Brothers, E. N.; Kudin, K. N.; Staroverov, V. N.; Keith, T. A.; Kobayashi, R.; Normand, J.; Raghavachari, K.; Rendell, A. P.; Burant, J. C.; Iyengar, S. S.; Tomasi, J.; Cossi, M.; Millam, J. M.; Klene, M.; Adamo, C.; Cammi, R.; Ochterski, J. W.; Martin, R. L.; Morokuma, K.; Farkas, O.; Foresman, J. B.; Fox, D. J. Gaussian, Inc., Wallingford CT, **2016**.

⁶⁰ Neese, F. The ORCA program system. *WIREs Comput Mol Sci* **2012**, *2* (1), 73–78 DOI: 10.1002/wcms.81.

⁶¹ Neese, F. Software update: the ORCA program system, version 4.0. *WIREs Comput Mol Sci* **2018**, *8* (1), e1327 DOI: 10.1002/wcms.1327.

⁶² Grochala, W.; Hoffmann, R.; Feng, J.; Ashcroft, N. W. The Chemical Imagination at Work InVery Tight Places. *Angewandte Chemie International Edition* **2007**, *46* (20), 3620–3642. <https://doi.org/10.1002/anie.200602485>.

⁶³ Pierotti, R. A. A Scaled Particle Theory of Aqueous and Nonaqueous Solutions. *Chemical Reviews* **1976**, *76* (6), 717–726. <https://doi.org/10.1021/cr60304a002>.

⁶⁴ Hoffmann, R.; Woodward, R. B. Orbital Symmetries and Endo-Exo Relationships in Concerted Cycloaddition Reactions. *J Am Chem Soc* **1965**, *87* (19), 4388–4389. <https://doi.org/10.1021/ja00947a033>.

⁶⁵ (1) Yu, P.; Patel, A.; Houk, K. N. Transannular [6 + 4] and Ambimodal Cycloaddition in the Biosynthesis of Heronamide A. *J Am Chem Soc* **2015**, *137* (42), 13518–13523. <https://doi.org/10.1021/jacs.5b06656>.

⁶⁶ (1) Yu, P.; Chen, T. Q.; Yang, Z.; He, C. Q.; Patel, A.; Lam, Y.; Liu, C.-Y.; Houk, K. N. Mechanisms and Origins of Periselectivity of the Ambimodal [6 + 4] Cycloadditions of Tropone to Dimethylfulvene. *J Am Chem Soc* **2017**, *139* (24), 8251–8258. <https://doi.org/10.1021/jacs.7b02966>.

⁶⁷ (1) Chen, S.; Yu, P.; Houk, K. N. Ambimodal Dipolar/Diels–Alder Cycloaddition Transition States Involving Proton Transfers. *J Am Chem Soc* **2018**, *140* (51), 18124–18131. <https://doi.org/10.1021/jacs.8b11080>.

-
- ⁶⁸ (1) Chen, S.; Yu, P.; Houk, K. N. Ambimodal Dipolar/Diels–Alder Cycloaddition Transition States Involving Proton Transfers. *J Am Chem Soc* **2018**, *140* (51), 18124–18131. <https://doi.org/10.1021/jacs.8b11080>.
- ⁶⁹ (1) Liu, F.; Chen, Y.; Houk, K. N. Huisgen's 1,3-Dipolar Cycloadditions to Fulvenes Proceed via Ambimodal [6+4]/[4+2] Transition States. *Angewandte Chemie Int Ed* **2020**, *59* (30), 12412–12416. <https://doi.org/10.1002/anie.202005265>.
- ⁷⁰ (1) Jamieson, C. S.; Sengupta, A.; Houk, K. N. Cycloadditions of Cyclopentadiene and Cycloheptatriene with Tropones: All Endo-[6+4] Cycloadditions Are Ambimodal. *J Am Chem Soc* **2021**, *143* (10), 3918–3926. <https://doi.org/10.1021/jacs.0c13401>.
- ⁷¹ (1) Zhang, H.; Thøgersen, M. K.; Jamieson, C. S.; Xue, X.-S.; Jørgensen, K. A.; Houk, K. N. Ambimodal Transition States in Diels–Alder Cycloadditions of Tropolone and Tropolonate with N-Methylmaleimide. *Angewandte Chemie Int Ed* **2021**. <https://doi.org/10.1002/anie.202109608>.
- ⁷² Yang, T.; Fukuda, R.; Cammi, R.; Ehara, M. Diels–Alder Cycloaddition of Cyclopentadiene and C60 at the Extreme High Pressure. *J Phys Chem* **2017**, *121* (22), 4363–4371. <https://doi.org/10.1021/acs.jpca.7b02805>.
- ⁷³ Chen, B.; Crespi, V.; Hoffmann, R. Theoretical Studies of Furan and Thiophene Nanowires: Structures, Cycloaddition Barriers and Activation Volumes. *ChemRxiv* **2021**. <https://doi.org/10.26434/chemrxiv.14347163.v2>. This content is a preprint and has not been peer-reviewed.
- ⁷⁴ Hammond, G. S. A Correlation of Reaction Rates. *J Am Chem Soc* **1955**, *77* (2), 334–338. <https://doi.org/10.1021/ja01607a027>.